JTTEE5 18:996–1003
DOI: 10.1007/s11666-009-9396-0
1059-9630/$19.00 © ASM International

Modeling the Build-Up of Internal Stresses in Multilayer Thick Thermal Barrier Coatings

H. Samadi and T.W. Coyle

(Submitted January 30, 2009; in revised form August 6, 2009)

Of the many factors affecting the durability and failure mechanisms of thermal spray coatings, in-service and residual stresses play an especially important role as the thickness of the coating increases. In this study, a numerical model for calculating the evolution of stresses within a multilayer coating during deposition is introduced. Model calculations are then validated by comparison with temperature and curvature measurements made during coating deposition.

Keywords internal stresses, multilayer ceramic coating, plasma-sprayed coating, quenching stress, stress modeling, thermal barrier coating, thermal stress

1. Introduction

One of the most important parameters controlling the durability of plasma spray coatings is the residual stress (Ref 1). The stress state of a coating in-service depends on both the residual stresses present after fabrication and the stresses arising from the mechanical and thermal loads arising from the service conditions. The residual stresses that are induced in the fabrication process may contribute directly to mechanical failure of the coating. For example, delamination may occur along the interface of pre-tensioned coatings (Ref 2) while compressive residual stress may cause spalling inside the coating (Ref 3). Thick coatings are especially prone to cracking and delamination near the coating-substrate interface due to the mismatch in thermomechanical properties between the top coat and the substrate (Ref 4). Thick coatings also experience higher stresses in-service under both steady state and transient heating (Ref 4).

According to numerical calculations, when a liquid droplet hits the substrate, it cools from the temperature of the molten droplet in-flight to the substrate temperature in a time of the order of microseconds (Ref 5, 6). The shrinkage associated with cooling the newly formed splat from the melting (solidification) temperature to the substrate temperature is constrained by the attachment of the newly solidified splat to the substrate, resulting in the formation of a tensile stress within individual splats known as the quenching stress (Ref 1, 7).

For a typical ceramic material (e.g., alumina), the maximum predicted quenching stress exceeds 1 GPa, although experimental studies show a value on the order of tens of MPas (Ref 1). There are two main reasons for this huge difference: one is that stress build up would not start while the particle temperature is still close to the melting point due to rapid stress relaxation by diffusive processes. Thus, a temperature called the creep temperature is employed to define the cooling range instead of the melting point. This temperature is the lowest temperature at which the creep rate is significant in the material. For mullite this temperature is about 1000 °C (Ref 8). Secondly, these stresses may be relaxed by plastic deformation in metallic materials and formation of microcracks in individual splats perpendicular to the splat boundaries in ceramics (Ref 6, 9).

The stresses referred to here as thermal stresses are generated when a system at a uniform initial temperature cools to a uniform final temperature (Ref 7). These stresses are due to a mismatch in the coefficient of thermal expansion (CTE) between the coating and the substrate. Macroscopic stresses that occur between the coating and the substrate are of interest due to their effect on adhesion of the coating (Ref 6) and their role in determining coating durability.

2. Previous Models

Many studies have modeled thermal stresses in duplex and multilayer coating-substrate systems (Ref 1, 7, 8, 10-21). In predicting the internal stresses, various simplifying assumptions are often made to balance the complexity of the analysis with the objectives of the study and the thickness and structure of the coating. For example, the coating may be assumed thin relative to the substrate; uniform temperatures may be assumed through the thickness of the coating and substrate; the quenching stress may or may not be considered.

The residual stress due to differences in the CTE between the coating and substrate (and between layers in a multilayer coating) when cooled from a stress-free state at the deposition temperature to room temperature has been

H. Samadi and **T.W. Coyle**, Centre for Advanced Coating Technologies, University of Toronto, Toronto, ON, Canada. Contact e-mail: hamed.samadi@utoronto.ca.

analyzed in many studies. Teixeira (Ref 12, 13) calculated the residual stress in thin multilayer PVD coatings numerically. This model assumed a constant stress within each individual layer appropriate for thin layers not for thick thermal spray deposits. Jin et al. (Ref 16, 17) modeled transient thermal stresses in the vicinity of a crack in functionally graded coatings. Their model also calculated the stress distribution in the coating under service conditions. In the stress calculations performed by Steffens et al. (Ref 6, 10) to determine the influence of thermal stresses on the thermal shock resistance of yttria-stabilized zirconia thermal barrier coatings, the simplified equation employed did not consider the substrate rigidity, the Poisson ratio of the substrate, or the coating thickness. Levine et al. (Ref 11) reported results from Dietzel that used a more complete equation, which overcame many of the limitations of Steffen's work.

Fewer publications attempt to address the pass-by-pass nature of the build-up of thermal spray coatings. Kesler et al. (Ref 21) described an analytical technique to determine the modulus of elasticity (E), coefficient of thermal expansion (α) and the quenching stress and thermal stress contributions to the residual stress of a Ni-Al_2O_3 functionally graded coating by measuring the curvature of a series of specimens with a range of coating thickness. The most complete predictive model to date has been that of Gill and Clyne (Ref 7, 22) who developed a numerical simulation coded in Lightspeed Pascal™ to calculate the temperature distribution and internal stress development of plasma-sprayed coatings during a pass-by-pass deposition process. This simulation considered the heating of the substrate and previously deposited material due to heat transfer from the torch, and clearly showed the importance of including the quenching stress in the total residual stress after cooling to room temperature. To make the pass-by-pass modeling approach more accessible, Tsui and Clyne developed an analytical version for planar and cylindrical geometries (Ref 18-20). In this analytical model, the modulus of elasticity, Poisson's ratio, and the CTE for the previously deposited material were estimated by a rule of mixtures approach. The temperature of the substrate and previously deposited layers was assumed to remain constant as the coating was built up. An analytical code based on this model is available (Ref 23) and will be used as a basis of comparison with the numeric calculations described later. Zhang et al. (Ref 14, 15) derived an analytical model to calculate the evolution of the internal stress in a functionally graded coating as the coating was built-up pass by pass. This model did not include the effects of the quenching stress and was not validated by comparison with experimental results.

In the current study, a commercially available finite element analysis program (Ref 24) was employed to model the temperature distribution and internal stresses developed during the pass-by-pass plasma spray deposition of a thick multilayer coating, including both the quenching stress and thermal stress contributions. The objective was to employ readily available numerical modeling software to avoid simplifying assumptions incorporated in the analytical models described above (Ref 14, 15, 18-20). The results of the model were used to predict the curvature of thin substrate specimens during coating deposition. The predicted curvatures were then compared to experimental observations.

3. Modeling

During plasma spray deposition, the plasma torch traverses back and forth across the substrate, depositing a layer of coating (a pass) on the substrate. The thickness of a pass is on the order of ~10 μm. The model approximates the continuous build-up of a plasma sprayed coating by the sequential addition of separate layers on top of previously deposited material, each new layer representing one pass. The thickness of each pass and the frequency at which passes are added are chosen to correspond to typical deposition parameters.

Two sources of internal stress are considered in the model. The first is the stress related to the cooling of the most recent pass to the temperature of the previously deposited material and substrate, i.e. the quenching stress. The second is the cooling of the entire coating and substrate to room temperature, i.e. the thermal stress.

A commercial finite element modeling software package (Comsol Multiphysics, Comsol, Inc., Burlington, MA, USA) was used to model the physics of heat transfer and the structural mechanics. The heat transfer part was solved first. The resulting temperature distributions were then used in the structural mechanics part to calculate the local strains and the curvature. The major assumptions involved in the simulation are given subsequently.

The deposition rate is less than the solidification rate. Thus, each new pass is deposited onto solidified material. This is consistent with a solidification time for individual splats of <10 μs, the time between successive splat impacts during a single pass of 1-100 μs, and a time between passes of >10 ms (Ref 25).

Each pass arrives as a thin layer covering the entire substrate at the same time. The thickness is based on dividing the thickness of the coating obtained in related experimental trials by the number of passes.

A delay is assumed between the arrivals of two passes, approximately equal to the time required for the torch to return to a given point on the sample during experimental trials.

During the deposition stage, the front surface of the sample is heated by conduction from the newly arrived pass, assumed to be 100 °C above its melting point, and by the hot plasma gas through convection. As the gun is close to the coating, convective heat absorption from the plasma jet dominates the heat loss from the front face. Heat is lost from the back surface of the substrate by convection. Heat transfer by radiation from the back surface of the substrate to the ambient was estimated to be two orders of magnitude lower than convection and four orders of magnitude lower than conduction from the top coat to the substrate and therefore not included in the calculation.

During the cooling stage, heat is lost from the front and back surfaces of the sample by convection.

During the deposition stage, the temperature distribution, internal strains, and the resulting curvature are calculated at the end of the delay after each pass. During the cooling stage, the temperature distribution is calculated at 3-s intervals. Then, the internal strains and curvature arising from the temperature gradients and differences in CTE during cooling are added to the pre-existing strain distribution and curvature generated during the pass-by-pass coating build-up.

For the numerical calculations reported here, the model parameters were selected to correspond with the experiments described in the following section. The substrate was a steel strip with dimensions of 100 × 10 × 3 mm ($l \times w \times t$). A 3-s delay was assumed between the arrivals of two passes, and a 20 μm layer thickness was used corresponding to the deposition conditions employed.

The mechanical boundary conditions and mesh geometry are shown in Fig. 1. The bottom was fixed, corresponding to experimental situation in which the sample clamped along its bottom edge. A Lagrange-Quadratic mesh was used, the default element type for mechanics analyses in this software (Ref 24). The automatic mesh refinement algorithm was used to set the element sizes within the substrate. The mesh size within each pass was set to the minimum value, which corresponded to 53,296 elements within the 20 μm thick passes. A total of 167,352 nodes were used for the thickest multilayer specimen modeled.

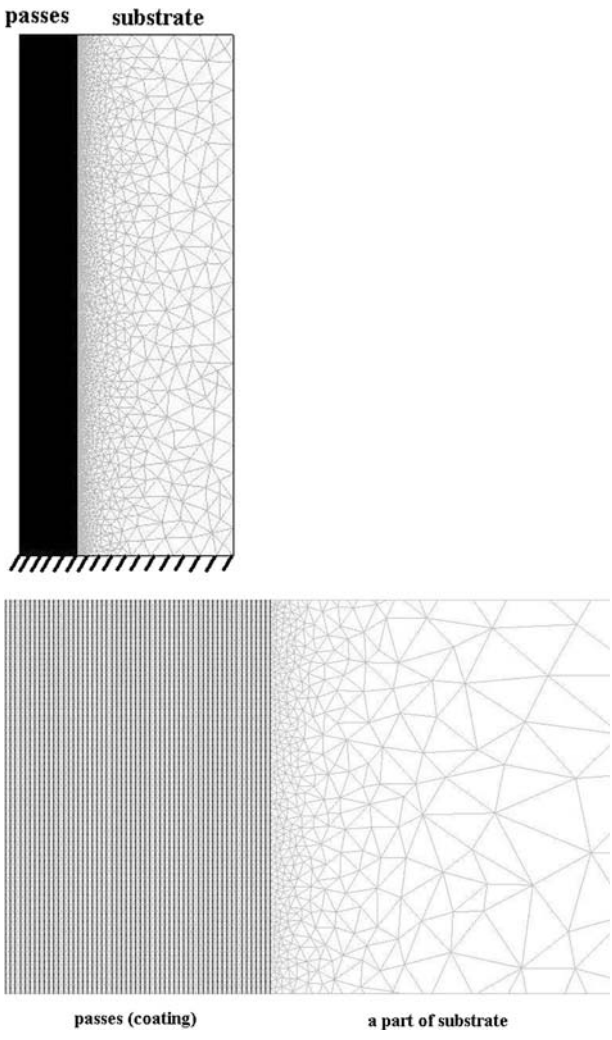

Fig. 1 Mechanical boundary conditions and mesh geometry

The thermal conductivity and modulus of elasticity of the coating materials are highly correlated to the amount and distribution of porosity in the coatings. The values employed for these properties were measured on coatings deposited under identical conditions, then released from the substrate using a 50 vol.% nitric acid − 50 vol.% water solution kept at 50 °C. Thermal diffusivity was measured with the laser flash method (Thermaflash 2200, Holometrix-Micromet, Inc., Bedford, USA) on 9 × 9 × 1.5 mm ($w \times l \times h$) samples. The elastic modulus was measured in 4-point bending using specimens 50 × 15 × 4 mm with inner and outer spans of 20 and 40 mm. A strain gauge (3 × 9 mm) was bonded to the central area of the tensile surface of the specimen to measure the strain during loading of the sample.* Literature values were used for the other material properties, as listed in Table 1. The temperature dependence of the substrate modulus of elasticity and of the thermal conductivities of the substrate and the coating are included.

The heat transfer coefficients for the back surface of the substrate/ambient air interface and the front surface/plasma gas interface are needed. For the substrate/ambient air interface, the heat transfer coefficient was chosen such that during cooling the simulation of the forsterite deposition (first layer) reached room temperature at the same time as in the experiment. Heat transfer by radiation from the back surface of the substrate to the ambient was estimated to be two orders of magnitude lower than convection and four orders of magnitude lower than conduction from the top coat to the substrate and therefore not included in the calculation. The heat transfer coefficient for the top surface/plasma gas interface was chosen from a literature report (Ref 26). The temperature of the plasma gas impinging on the coating surface was set to a temperature which gave the same temperature as measured for the first pass deposition of forsterite. These values were then utilized throughout the modeling (Table 2).

4. Experimental Approach

Among techniques for measuring residual stresses in materials, in situ curvature measurement using a linear

*Detaching the coating from the substrate will change the level of residual stress present in the coating. If the modulus of elasticity depends on the level of residual stress, the modulus measured for the detached coating may differ from the modulus exhibited by the coating while attached to the substrate.

Table 1 Material properties used in the model

Material properties	Stainless steel (Ref 24)	NiCrAlY (Ref 26)	YSZ (Ref 26)	Forsterite	Spinel	Mullite
Modulus of elasticity (GPa)	205	64.5	13.6	12.3 (a)	26.7 (a)	19 (a)
Poisson's ratio	0.33	0.30	0.25	0.24 (Ref 27)	0.29 (Ref 27)	0.25 (Ref 28)
Thermal conductivity (W/mK) @ RT	44.5	3.88	0.67	1.98 (a)	5.12 (a)	1.29 (a)
Coefficient of thermal expansion ($\times 10^{-6}$ K^{-1}) @ RT	12.3	10.3	7.5	11 (Ref 27)	7.68 (Ref 27)	5.1 (Ref 28)
Density (kg/m^3)	7850	6290	5600	2020 (a)	3060 (a)	2710 (a)
Specific heat (J/kg K) @ RT (Ref 29)	475	460	420	830	820	760

YSZ, yttria stabilized zirconia
(a) Experimentally measured

Table 2 Values used in heat transfer physics

	Heat transfer coefficient, W/m^2 K	Ambient temperature, K
Air jet at the back of the substrate	50	300
Plasma gas	320	4000

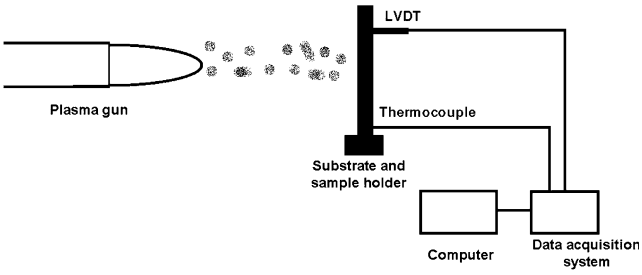

Fig. 2 Schematic illustration of the continuous curvature measurement setup

variable differential transformer (LVDT) (Solarton Metrology, Forestville, NY, USA) was chosen for this study. This method was utilized for this purpose before (Ref 27, 28). To have a better understanding of the stress build up, each layer was separately deposited according to the chosen parameters and curvature was measured continuously.

A schematic of the setup for curvature measurement is shown in Fig. 2. The substrate is a strip of stainless steel with dimensions of 100 × 10 × 3 mm ($l \times w \times t$). The core of the LVDT is in contact with the back of the substrate via a quartz rod (to prevent overheating). A data acquisition system records the horizontal movements of the substrate. The temperature of the back of the substrate is also measured using a thermocouple in contact with the substrate through a data acquisition system. Two air jets are directed at the back of the substrate to prevent the substrate from over-heating and simulate a real deposition configuration. In spraying thick ceramic coatings, the substrate is cooled from the back to prevent substrate over heating due to prolonged spraying time. The robotic arm moves the torch up and down at a constant speed of 70 mm s^{-1} (Fig. 3).

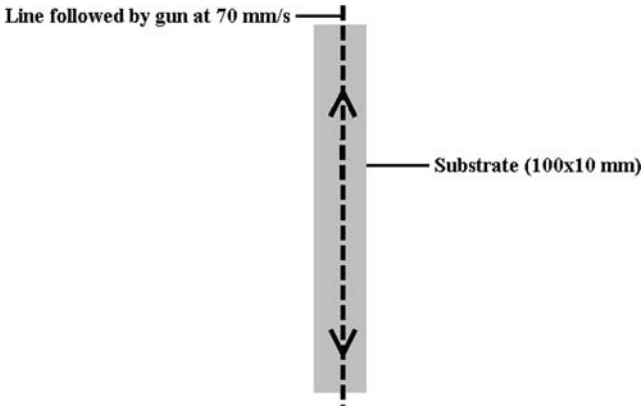

Fig. 3 Schematic diagram showing spray pattern of the gun

Table 3 Spraying parameters

Parameter	Coating		
	Forsterite	Spinel	Mullite
Current, A	340	700	600
Primary gas flow rate, L/min	CO_2-60	Ar-70	Ar-70
Secondary flow rate, L/min	CH_4-30	H_2-1	H_2-5
Standoff distance, mm	75	75	100
Feeding rate, g/min	10	10	10
Carrier gas flow rate, L/min	10	10	10

The width of the substrate was chosen to be wide enough to minimize edge effects, but narrow enough to allow a uniform coating thickness to be deposited. Prior to coating, the substrate was grit-blasted to increase the bonding with the coating. This treatment results in a compressive stress at the surface of the substrate that causes bending. To remove this curvature, the opposite face of the substrate was grit-blasted until the substrate became flat.

First, single layer coatings of forsterite, spinel, and mullite were deposited on the stainless steel substrates employing the deposition process parameters given in Table 3. Multilayer coatings were made by depositing each layer to the desired thickness, allowing the coating and substrate to cool to room temperature and then depositing the next layer on top of it. A 200 μm layer of forsterite was sprayed and cooled to room temperature

followed by a 50 μm spinel layer and a 750 μm mullite layer, again using the process parameters in Table 3.

5. Results and Discussion

As mentioned earlier, the temperature of the back of the substrates was measured in real time while spraying forsterite coatings. These experimental data were used to validate the thermal part of the numerical calculations. Figure 4 shows the results of experiments and calculations for three samples. The continuous lines are the experimental results. The calculated temperatures are shown with dots. The substrate was not preheated in these experiments in order to more effectively assess the ability of the simulation to predict temperature changes during deposition. The large fluctuations in the measured temperature reflect the motion of the torch from the top to the bottom of the substrate where the thermocouple was located. Since the model assumes uniform heat transfer over the hot surface, it does not capture the rapid fluctuations in temperature. However, the average substrate temperature, predicted for all three coating materials using the values for the heat transfer coefficients and plasma gas temperature obtained by fitting to the initial forsterite results, agrees with the experimental measurements to within ~50 °C.

Curvature calculations for the multilayer coating are compared with the measured curvature in Fig. 5. The curvature at the beginning of deposition of the forsterite layer is zero, the state of the stress-free substrate. For the spinel and mullite layers, the initial curvature was the final curvature after cooling the previously deposited layer and substrate to room temperature. The model effectively predicts the curvature changes throughout the three deposition steps, including the intermediate cooling and reheating cycles. The fluctuations in the measured curvature beginning at ~300 s in the graph of the mullite deposition are due to the appearance of a large interfacial crack between the forsterite layer and the substrate, visible to the eye, which would have released a portion of the internal stresses.

During deposition the sample curved toward the torch, indicating tensile stresses are developed in the coating. The large variation in the measured curvature during deposition corresponds to motion of the torch from the top of the sample down to bottom (clamped) end of the specimen, and then back to the top. When the gas jet impinges on the top (free) end of the sample, the force of the jet bends the sample away from the torch, creating a negative curvature. As the torch moves toward the clamped end of the specimen that effect is nearly eliminated, and the curvature becomes more indicative of the internal stresses within the specimen. After the coating reached the desired thickness, the gun was shut down and the system cooled down to room temperature. During this stage, the temperature is nearly uniform through the thickness of the coating and substrate. The substrate shrinks more due to its higher CTE, and the sample straightens.

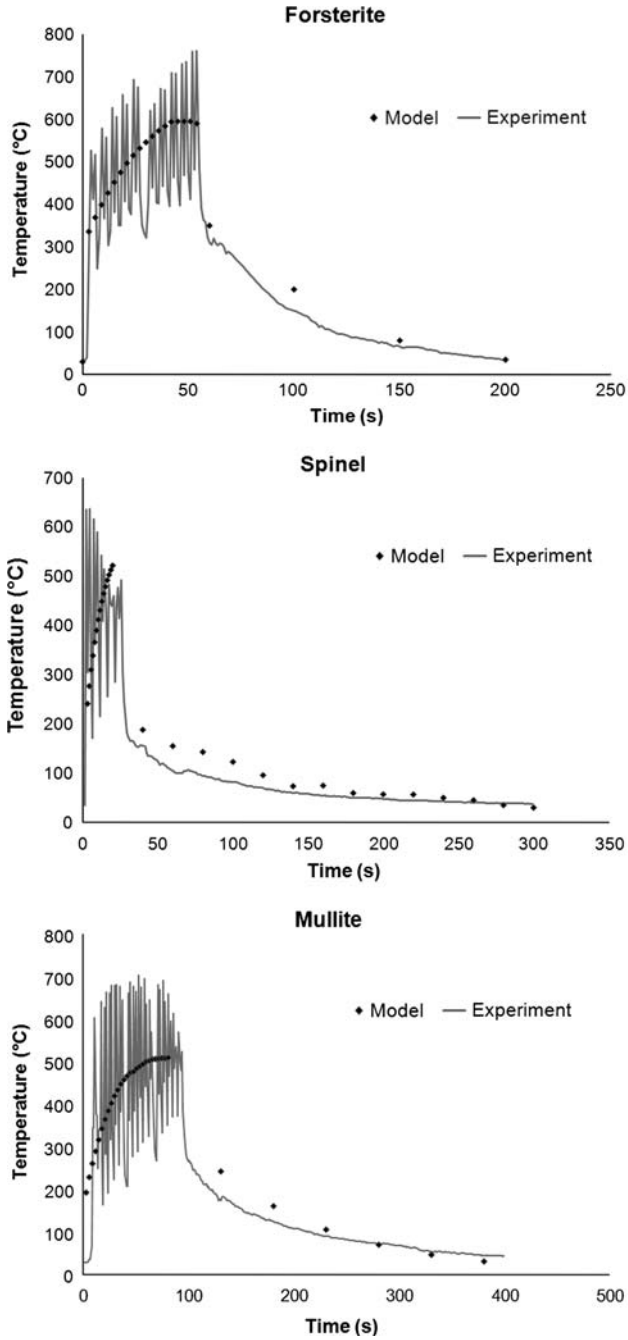

Fig. 4 Temperature of the back of the substrate during spraying: forsterite (top), spinel (middle), and mullite (bottom)

The model assumes that the quenching stress develops as the coating cools from its melting point to the substrate temperature. This is an upper bound estimate, since stress relaxation by rapid diffusion near the melting point and the formation of microcracks during cooling would tend to decrease the quenching stress (Ref 1). When the first pass arrives on the substrate, the substrate is at room temperature. As more passes are deposited, the substrate temperature increases and the temperature difference over

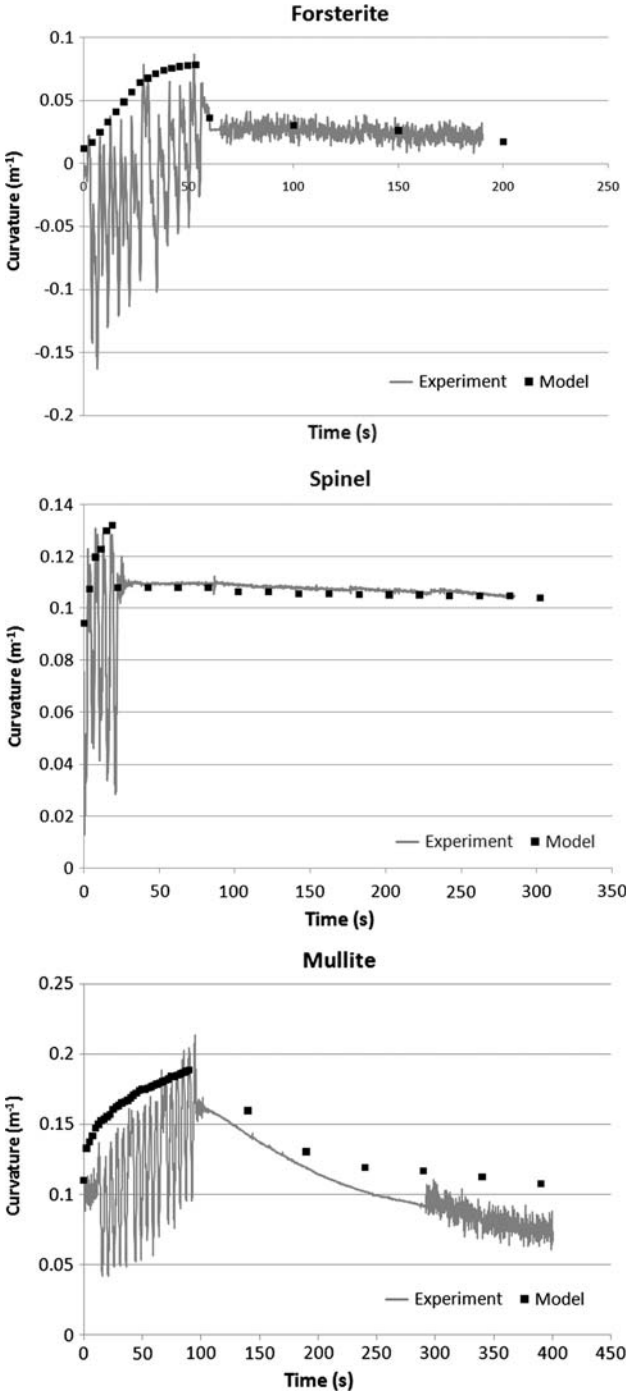

Fig. 5 Comparison of the measured curvature with that predicted by the numerical model during deposition of the multilayer coating: forsterite on the stainless steel substrate (top), spinel on the previously deposited forsterite layer (middle), and mullite on the spinal and forsterite layers (bottom)

which the quenching stress develop decreases. Thus, in the model the quenching stress in each pass decreases as additional passes are deposited. A second contribution to the initial curvature arises due to the increase in the substrate and coating temperature during deposition. The

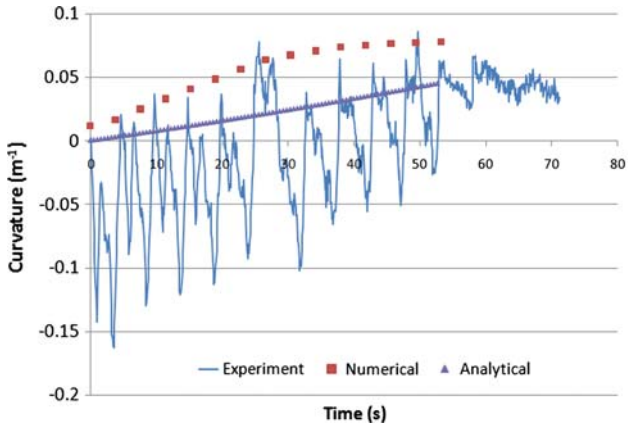

Fig. 6 The measured curvature during deposition of the forsterite coating compared with predictions of the current numerical model and calculations based on the analytical model of Tsui and Clyne (Ref 18-20)

coating deposited on the first pass cools to the substrate temperature, which is calculated to be ~200 °C at that point. As this first pass deposit heats up from ~200 to ~575 °C along with the substrate during deposition of subsequent passes, the difference in CTE between the coating and substrate would increase the tensile stress in that first pass deposit, contributing to the curvature toward the torch. This effect would also decrease for each subsequent pass.

The curvature measured during the deposition of forsterite is compared in more detail with the numerical model and the results of the analytical solution of Tsui and Clyne (Ref 18-20) in Fig. 6. As discussed earlier, the peak in the fluctuations is believed to best describe the curvature due to the internal stresses. The numerical model generally follows the envelope described by the peaks and predicts a non-linear increase in curvature with the number of passes due to the effects of the increase in temperature of the substrate (and any previously deposited passes) described earlier. In the analytical model, the substrate temperature was assumed to be constant (550 °C) during deposition, and the quenching stress chosen arbitrarily to be 80 MPa to yield agreement with the experimental data at the end of the deposition stage. Thus, the analytical model predicts a linear increase in curvature with the number of passes.

For a material with a large CTE mismatch with the substrate (e.g., mullite), the thermal stress (the stress generates while the coating is being cooled) is large compared to the quenching stress, and the effects of the quenching stress may then be negligible. However, for a material with a coefficient of thermal expansion close to that of the substrate (e.g., forsterite), this small quenching stress can be crucial in the sign of the final residual stress (tensile or compressive). This is illustrated in Fig. 7 where the through-thickness stress distribution predicted by the numerical model for a forsterite coating on stainless steel is again compared with the results of the analytical solution of Tsui and Clyne (Ref 18-20) and the curvature

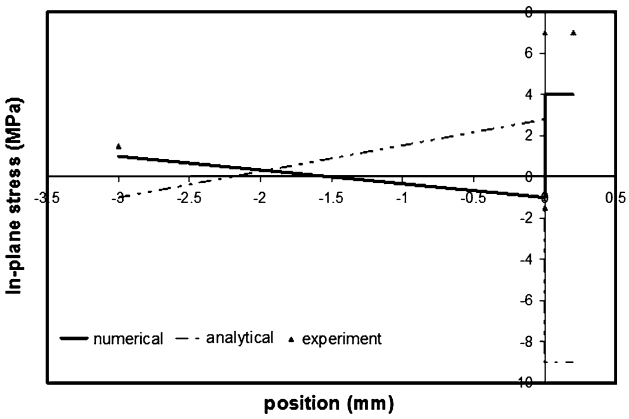

Fig. 7 Comparison of the in-plane stress distribution through the thickness of a forsterite coating and substrate calculated from the numerical model and analytical solution with the experimentally derived values after cooling to room temperature

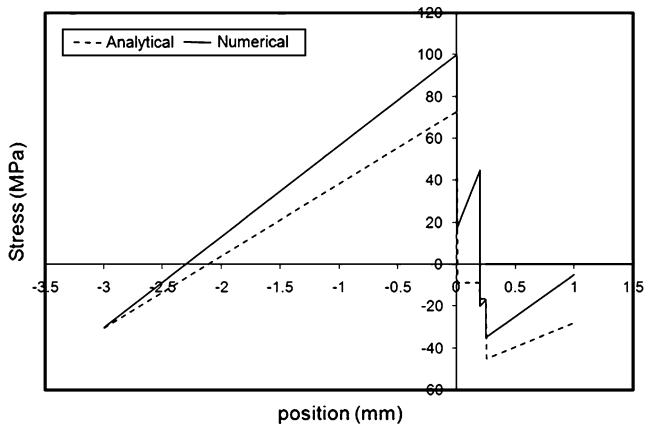

Fig. 8 Stress distribution through the thickness of the multilayer coating system as predicted by the current numerical model and the analytical model

determined experimentally at room temperature. In the analytical solution, the quenching stress was assumed to be negligible and the substrate temperature constant at 550 °C during deposition. Both the numerical simulation and the experimental result indicate that the stress in the coating is tensile, while the analytical result (assuming no quenching stress) predicts a compressive stress due to the difference in CTE between the coating and substrate.

The stress distribution through the thickness of the multilayer coating and stainless steel substrate after cooling to room temperature as predicted by the numerical model and calculation based on the Tsui and Clyne (Ref 18-20) model is shown in Fig. 8. The analytical model calculation assumed a constant substrate temperature of 600 °C during deposition, and a negligible quenching stress for all layers. The major differences are the stresses in the forsterite layer and mullite layer. The numerical model predicts a tensile stress in the forsterite layer while the analytical model predicts a small compressive stress. The stress in the mullite layer is predicted to be compressive in both cases, although the numerical model predicts that stress to be less than 10 MPa at the surface.

The results of the curvature measurements discussed previously indicated that the quenching stress may have a significant effect even for these brittle ceramic coatings. The assumption of a negligible quenching stress in the analytical model is therefore likely the main reason for the discrepancies in the two predictions for this multilayer coating system, although the analytical model also neglects the effects of any temperature changes which may occur during deposition and the temperature dependence of material properties. The straightforward numerical model described here avoids such assumptions, often needed to make analytical models tractable. It demonstrates that the ease of use of current, commercially available finite element analysis software packages provides the capability to predict the build-up of internal stresses in multilayer coatings at a useful level of accuracy under realistic deposition conditions. This in turn points toward the ability to control internal stresses through appropriate design of coating architecture, microstructure, and deposition conditions (i.e., substrate temperature).

6. Conclusions

Residual stress is a main factor in the durability of plasma-sprayed coatings. The difference in the coefficient of thermal expansion of the coating and substrate (and of different coating layers) combined with the temperature evolution and temperature gradients in the coating and substrate during deposition largely determine the residual stress for a given set of material properties. This study reviews the existing models for the calculation of residual stresses in coatings. A numerical model was developed using a commercially available finite element analysis package that attempts to balance ease of use with the need to include consideration of several complex factors identified in previous work. The model accounts for the effects of the pass-by-pass deposition process on the evolution of temperature and stress within the coating and substrate. Model predictions were compared with experimental measurements of sample temperature and curvature during deposition of a multilayer coating. The model accurately predicted the observed behavior throughout the deposition process.

References

1. S. Kuroda and T.W. Clyne, The Quenching Stress in Thermally Sprayed Coatings, *Thin Solid Films*, 1991, **200**, p 49-66
2. K. Kokini, B.D. Choules, and Y.R. Takeuchi, Thermal Fracture Mechanisms in Ceramic Thermal Barrier Coatings, *J. Therm. Spray Technol.*, 1997, **6**, p 43-49
3. A.H. Bartlett and R. Dalmaschio, Failure Mechanisms of a Zirconia-8 wt% Yttria Thermal Barrier Coating, *J. Am. Ceram. Soc.*, 1995, **78**, p 1018-1024

4. S. Rangaraj and M. Kokini, Interface Thermal Fracture in Functionally Graded Zirconia-Mullite-Bond Coat Alloy Thermal Barrier Coatings, *Acta Mater.*, 2003, **51**, p 251-267
5. R. Dhiman, A.G. McDonald, and S. Chandra, Predicting Splat Morphology in a Thermal Spray Process, *Surf. Coat. Technol.*, 2007, **201**, p 7789-7801
6. R.B. Heimann, *Plasma-Spray Coatings: Principles and Applications*, VCH, 1996
7. S.C. Gill and T.W. Clyne, Stress Distributions and Material Response in Thermal Spraying of Metallic and Ceramic Deposits, *Metall. Trans. B*, 1990, **21**, p 377-385
8. K. Kokini, Y.R. Takeuchi, and B.D. Choules, Surface Thermal Cracking of Thermal Barrier Coatings Owing to Stress Relaxation: Zirconia vs Mullite, *Surf. Coat. Technol.*, 1996, **82**, p 77-82
9. M. Xue, J. Mostaghimi, and S. Chandra, Investigation of Splat Curling Up in Thermal Spray Coatings, *International Thermal Spray Conference*, B.R. Marple, M.M. Hyland, Y.C. Lau, R.S. Lima, and J. Voyer, Ed., May 15-18, 2006 (Seattle, WA), ASM International
10. H.D. Steffens, Z. Babiak, and U. Fischer, Influence of Residual and Thermal Stresses on the Thermal Shock Resistance of $ZrO_2.7Y_2O_3$ Thermal Barrier Coatings, *2nd International Conference on Surface Engineering* (Stratford-upon-Avon, Cambridge, UK), The Welding Institute, 1987, p 471
11. S.R. Levine, R.A. Miller, and M.A. Gedwill, Thermal Barrier Coatings Research at NASA Lewis, *Proceedings of the Second Conference on Advanced Materials for Alternate-Fuel Capable Heat Engines* (Monterey, CA, USA), 1982, p 006/185-006/204
12. V. Teixeira, Mechanical Integrity in PVD Coatings Due to the Presence of Residual Stresses, *Thin Solid Films*, 2001, **392**, p 276-281
13. V. Teixeira, Residual Stress and Cracking in Thin PVD Coatings, *Vacuum*, 2002, **64**, p 393-399
14. X.C. Zhang, B.S. Xu, H.D. Wang, Y. Jiang, and Y.X. Wu, Application of Functionally Graded Interlayer on Reducing the Residual Stress Discontinuities at Interfaces within a Plasma-Sprayed Thermal Barrier Coating, *Surf. Coat. Technol.*, 2007, **201**, p 5716-5719
15. X.C. Zhang, B.S. Xu, H.D. Wang, and Y.X. Wu, An Analytical Model for Predicting Thermal Residual Stresses in Multilayer Coating Systems, *Thin Solid Films*, 2005, **488**, p 274-282
16. Z.H. Jin and R.C. Batra, Stress Intensity Relaxation at the Tip of an Edge Crack in a Functionally Graded Material Subjected to a Thermal Shock, *J. Therm. Stress.*, 1996, **19**, p 317-339
17. Z.H. Jin and G.H. Paulino, Transient Thermal Stress Analysis of an Edge Crack in a Functionally Graded Material, *Int. J. Fract.*, 2001, **107**, p 73-98
18. Y.C. Tsui and T.W. Clyne, An Analytical Model for Predicting Residual Stresses in Progressively Deposited Coatings. 1. Planar Geometry, *Thin Solid Films*, 1997, **306**, p 23-33
19. Y.C. Tsui and T.W. Clyne, An Analytical Model for Predicting Residual Stresses in Progressively Deposited Coatings. 2. Cylindrical Geometry, *Thin Solid Films*, 1997, **306**, p 34-51
20. Y.C. Tsui and T.W. Clyne, An Analytical Model for Predicting Residual Stresses in Progressively Deposited Coatings. 3. Further Development and Applications, *Thin Solid Films*, 1997, **306**, p 52-61
21. O. Kesler, M. Finot, S. Suresh, and S. Sampath, Determination of Processing-Induced Stresses and Properties of Layered and Graded Coatings: Experimental Method and Results for Plasma-Sprayed Ni-Al_2O_3, *Acta Mater.*, 1997, **45**, p 3123-3134
22. S.C. Gill, ''Residual Stresses in Plasma Sprayed Deposits,'' Ph.D. Thesis, University of Cambridge, 1991
23. Composites and Coatings Group, and U.o. Cambridge, Coat Stress Planar Analyzer [online]. http://www.msm.cam.ac.uk/mmc/publications/software.html, 1998
24. COMSOL, COMSOL Multiphysics, 3.2 ed. [online]. http://www.comsol.com/products/multiphysics, 2005
25. P. Fauchais, Understanding Plasma Spraying, *J. Phys. D Appl. Phys.*, 2004, **37**, p R86-R108
26. H.W. Ng and Z. Gan, A Finite Element Analysis Technique for Predicting As-Sprayed Residual Stresses Generated by the Plasma Spray Coating Process, *Finite Elem. Anal. Des.*, 2005, **41**, p 1235-1254
27. S. Kuroda, T. Fukushima, and S. Kitahara, Simultaneous Measurement of Coating Thickness and Deposition Stress During Thermal Spraying, *Thin Solid Films*, 1988, **164**, p 157-163
28. S.C. Gill and T.W. Clyne, Investigation of Residual-Stress Generation During Thermal Spraying by Continuous Curvature Measurement, *Thin Solid Films*, 1994, **250**, p 172-180
29. R.H. Perry and D.W. Green, *Perry's Chemical Engineers' Handbook*, 8th ed., McGraw-Hill, 2008